Research Square

Preprints are preliminary reports that have not undergone peer review.
They should not be considered conclusive, used to inform clinical practice,
or referenced by the media as validated information.

Dual urease-CA profiling, optimization, and CaCO 3 biomineralization by environmental bacteria

Paul Mwangi
Cochin University of Science and Technology (CUSAT)
Vinod Kumar Nathan
CSIR – Central Food Technological Research Institute
Neenu Pavithran
Cochin University of Science and Technology (CUSAT)
Suhara Shebin
Cochin University of Science and Technology (CUSAT)
Parvathi Ammini
parvathi@cusat.ac.in
Cochin University of Science and Technology (CUSAT)

Research Article

Keywords: carbonic anhydrase, urease, calcium carbonate, microbial biomineralization, biocementation, zymography

Posted Date: November 12th, 2026

DOI: https://doi.org/10.21203/rs.3.rs-11458358/v1

License: This work is licensed under a Creative Commons Attribution 4.0 International License.
Read Full License

Additional Declarations: No competing interests reported.

Dual urease-CA profiling, optimization, and $CaCO_3$ biomineralization by environmental bacteria

Article type: Original Article

Paul Mwangi [1], Vinod Kumar Nathan[2], Neenu Pavithran[1], Suhara Shebin[1] and Parvathi Ammini [1]*

[1] Department of Biotechnology, Cochin University of Science and Technology (CUSAT), Kochi, Kerala, India.

[2] CSIR – Central Food Technological Research Institute, Mysore, Karnataka, India.

*Corresponding author

Dr Parvathi A

Professor and Head

Department of Biotechnology

Cochin University of Science and Technology

Kochi-682022, Kerala, India

Tel: +91-484-2575396, Fax: +91-484-2577595

Mob: 9847358540

Highlights

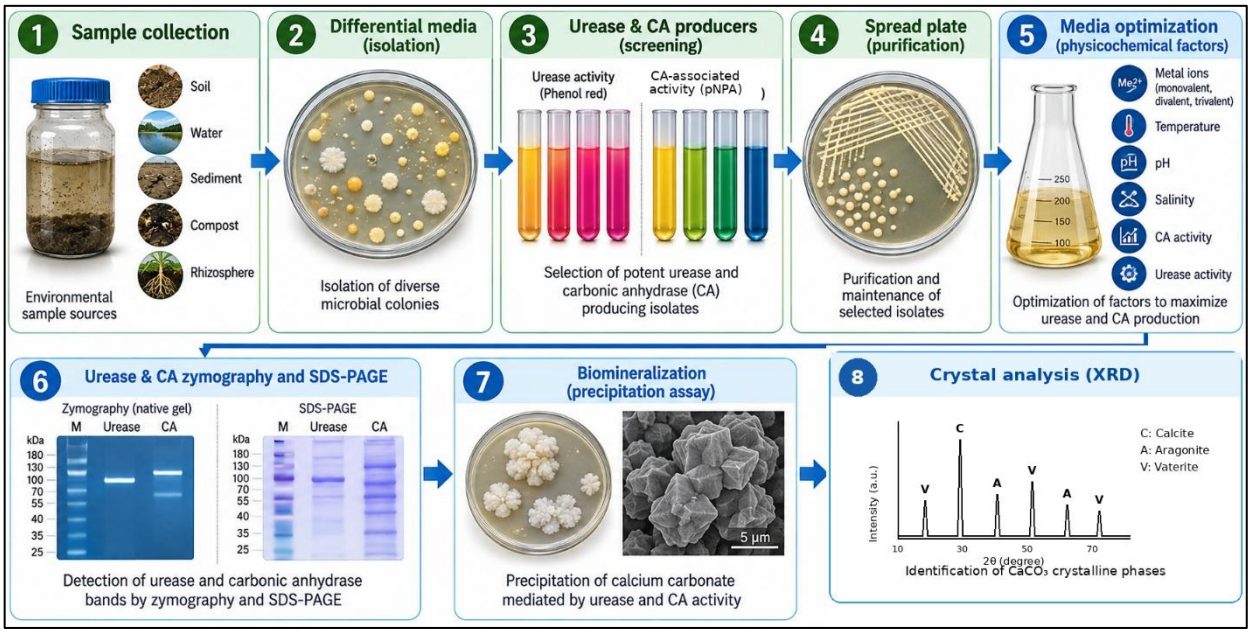
- Environmental bacterial isolates, LSI, SED and MS1, exhibited both urease and carbonic anhydrase-associated activities.
- LS1 showed the highest urease activity, whereas SED showed the highest CA-associated and CO_2-hydration activity.
- Peak responses generally occurred at 35 °C, pH 8, and 2% NaCl-supplemented LB medium.
- Genome annotation identified β-class carbonic anhydrase and *ureC* in all three isolates.
- Urease-mediated precipitation produced greater $CaCO_3$ yields than the CA-associated assay.
- SEM–EDX characterized mineral morphology and composition, while XRD identified calcite, vaterite, and aragonite.

Abstract

Microbially induced calcium carbonate precipitation (MICP) has mostly been studied through the ureolytic pathway, while carbonic anhydrase (CA)-assisted CO_2 hydration is typically examined separately. We screened 50 environmental bacterial isolates to identify dual enzyme activity. Three high-activity isolates (MS1, LS1, and SED) underwent phenotypic, biochemical, enzymatic, mineralogical, and partial 16S rRNA analysis. MS1 and LS1 were identified as *Lysinibacillus spp*., and SED as *Bacillus sp*. Growth and enzyme activities were evaluated across various environmental conditions. All 21 condition–response models showed significant effects of the tested variables. Optimal conditions were 35 °C, pH 8, 2% NaCl, LB medium, ~4 mM KCl, and 2% inoculum. Under these, LS1 showed the highest urease activity (31.3 U/mL), SED showed the highest CA-associated esterase activity (4.1 U/mL). Urease-mediated $CaCO_3$ production was highest in LS1 (5.35 g/L) and MS1 (5.32 g/L); CA-associated $CaCO_3$ was highest in MS1 (1.19 g/L). CO_2-hydration activity (WAU/mg) was greatest in SED (44.4), followed by LS1 (26.6) and MS1 (23.8). Zymography confirmed both enzyme activities, and genome annotation supported relevant gene presence (predicted β-class CA and UreC proteins). SED had the highest biofilm biomass but lowest mineral

yield, suggesting no direct correlation among biofilm formation, enzyme activity, and mineral production. Microscopy, SEM–EDX, and XRD identified calcite, vaterite, and aragonite. While the isolates showed dual enzyme capability, synergy remains unconfirmed as the pathways were assessed independently.

Graphical Abstract



Keywords: carbonic anhydrase; urease; calcium carbonate; microbial biomineralization; biocementation; zymography

1. Introduction

Microbially induced calcium carbonate precipitation (MICP) is a biologically driven mineralization process in which microbial metabolism generates carbonate species that react with calcium ions to form calcium carbonate ($CaCO_3$). Microbial cells and extracellular surfaces can also provide nucleation sites, allowing precipitation to proceed under comparatively mild conditions. MICP has attracted interest for applications in soil stabilization, biocementation, concrete crack repair, contaminant immobilization, carbon mineralization, and the rehabilitation of degraded infrastructure *(1, 2, 3)*. Its engineering performance depends not only on the amount of $CaCO_3$ formed, but also on where the mineral is deposited, its morphology and polymorphic composition, and the environmental tolerance of the producing microorganisms *(4,5)*.

The most well-established route to MICP is ureolysis. Urease is a nickel metalloenzyme that hydrolyses urea to ammonia, which raises alkalinity and leads to greater concentration of carbonate and precipitation of calcium carbonate. The rapid reaction can result in the production of high mineral quantities and has therefore been used extensively in biocementation systems *(6,7,8)*. However, high ureolysis rates may lead to localized mineral deposits and generate ammonium-polluted effluent that imposes practical and environmental limits on larger-scale treatment *(9)*.

An alternative biomineralization pathway is mediated by carbonic anhydrase (CA), a zinc-containing metalloenzyme that catalyses the reversible hydration of CO_2 to bicarbonate and protons. It plays a key role in inorganic carbon metabolism *(10,11)*. In alkaline, calcium-rich systems, the CA-induced increase in bicarbonate supply can lead to carbonate precipitation. Unlike ureolysis, CA-mediated mineralization offers the additional advantage of directly coupling CO_2 capture with carbonate formation, making it an attractive strategy for carbon sequestration. Recent studies have demonstrated the feasibility of CA-producing bacteria for soil biocementation and CO_2-to-$CaCO_3$ conversion *(12,13)*. Additionally, it is well established that the mineralization pathway can be

influenced by environmental conditions, with organisms such as *Bacillus megaterium* preferentially mineralize CA under specific growth conditions *(14)*.

Both enzymes have been found to contribute to carbonate production, but most studies are optimized independently for urease and CA. Consequently, little is known about naturally occurring bacterial isolates capable of expressing both enzymatic activities and their relative contributions to biomineralization under comparable conditions. The coexistence of urease and CA within a single organism does not necessarily imply synergistic mineralization, as the two pathways may respond differently to environmental factors and contribute independently to carbonate formation. Therefore, quantification of both activities, their environmental optima, and the link between the enzymatic phenotype and mineral yield and phase composition is important.

In the present study, environmental bacterial isolates were screened for both urease and carbonic anhydrase activities to identify strains possessing dual biomineralization potential. The precipitates were analyzed by light microscopy, scanning electron microscopy (SEM), energy-dispersive X-ray spectroscopy (EDX), and X-ray diffraction (XRD). Environmental factors influencing bacterial growth and enzyme production were optimized, and the contributions of urease- and CA-mediated pathways to calcium carbonate precipitation, carbon sequestration, and crystal polymorphism were evaluated independently. The confirmatory genomic analysis identified the presence of both carbonic anhydrase and urease genes in the selected isolates.

2. Materials and methods

2.1. Study design and sample collection

Samples (water, soil, sand, sewage, and waste) were collected aseptically from 11 locations in Ernakulam district, Kerala, India. Samples were transported in sterile containers to the laboratory for bacterial isolation. The sampling sources, collection locations, and geographical coordinates are presented in supplementary Table 1.

2.2. Preliminary enzyme screening

Serially diluted suspensions (~10^4–10^5) were added to the nutrient agar containing 0, 3, 5, 7, and 10 mM p-nitrophenyl acetate (pNPA) supplemented media and then incubated at 37 °C in order to test the ability of bacterial isolates to survive on pNPA-supplemented media. Based on retained growth, 3 mM pNPA was used for isolation. Colonies that were morphologically distinct were purified by repeated streaking and stored on LB agar slants. The accumulation of yellow color was measured as the hydrolysis of pNPA. As pNPA can be hydrolysed by other enzymes, this test was only used as an indicator and was additionally confirmed by CA esterase assays, protonography, CO_2-hydration measurements, and final confirmation of the presence of urease and carbonic anhydrase genes *(15,16)*. Urease activity was tested in urea broth. Sterile basal medium was supplemented with filter-sterilized 40% (*w/v*) urea solution. The isolates were cultured at 37 °C for a maximum of 72 h, and a positive urease reaction was noted from a colour change in phenol red due to the production of ammonia and the increase in pH.

2.3. Morphological and biochemical characterization

Colony morphology and Gram stain were used to characterize purified isolates, as well as Schaeffer–Fulton endospore stain and a hanging-drop motility test. The DNase activity was detected on methyl-green DNase agar after 72 hours of incubation at 37 °C. Selected isolates were differentiated based on oxidase, starch hydrolysis, and cyclodextrin glucanotransferase.

2.4. Preparation of crude enzyme extracts and protein determination

A pure isolate was streaked onto LB agar, and a single colony was grown in sterile LB broth (20 mL) at 37 °C for 24 h to make the mother culture. A 2% (*v/v*) inoculum from this culture (OD_{600} = 1.0 ± 0.2) was added to 500 mL of sterile LB broth in a 500 mL Erlenmeyer flask, incubated for 48 h at 37 °C at 150 rpm. After incubation, the cells were separated by centrifugation at 12,000 rpm for 10 min at 4 °C. The cell pellet was resuspended in 50 mM Tris-HCl lysis buffer (pH 8.3). Cell disruption was done by sonication. Cell debris was removed by centrifuging the resulting lysate at 12000 rpm for 10 min at 4 °C. The supernatant was collected as the intracellular crude enzyme fraction and stored at −20 °C for further analysis *(17)*.

Protein content was measured by the Bradford dye-binding method using bovine serum albumin (BSA) as the protein standard *(18)*. Calibrations were made from concentrations between 0–2500 μg mL^{-1}. 10 μL of the standard or sample was added to 190 μL of Bradford reagent, incubated at room temperature for 5 minutes, and measured at 595 nm. Triplicate measurements were made.

2.5. Urease activity assay

Urease activity was measured using the phenol–hypochlorite method based on modified Steyert and Kaper *(19)*. A 10 mM NH_4Cl stock solution was diluted to a 1 mM working solution, from which standards of 0, 200, 400, and 600 μM were prepared. For each assay, 50 μL of crude enzyme was mixed with 450 μL of 100 mM urea prepared in 20 mM phosphate buffer (pH 8.0) and incubated at 37 °C for 10 min. A 30 μL aliquot was then transferred to a microplate well, followed by 100 μL of phenol–hypochlorite reagent and 100 μL of sodium nitroprusside reagent. After incubation at 50 °C for 5 min, absorbance was measured at 630 nm. Ammonia release was determined from the NH_4Cl standard curve, and urease activity was expressed as U mL^{-1}

2.6. Carbonic anhydrase-associated assays

2.6.1. Esterase assay

Esterase activity in pNPA was used to measure CA activity. Reactions were performed with 20 μL of crude enzyme, 160 μL of 20 mM phosphate buffer (pH 7.4), and 20 μL of 3 mM pNPA in acetonitrile. After 5-8 min, the absorbance at 348 nm was measured, and the activity was calculated by measuring the amount of p-nitrophenol produced. Although the assay is based upon the known esterase activity of CA, when applied to crude extracts, it is not enzyme-specific, and the results are termed CA-associated esterase activity, except when substantiated by orthogonal evidence *(15)*.

2.6.2. Electrometric CO_2-hydration assay

A modified Wilbur–Anderson electrometric assay *(20, 21)* was used to determine carbon dioxide sequestration. CO_2-saturated water was freshly prepared by bubbling CO_2 into chilled, sterile water for 2 hours and then kept on ice. Crude enzyme extract (0.1 mL) was added to a chilled vessel containing 6.0 mL of 20 mM Tris–HCl (pH 8.3). This reaction was initiated with 4.0 mL of chilled

160 CO_2-saturated water, and the time required for the pH to drop from 8.3 to 6.3 was recorded. A no-
161 enzyme blank was used to estimate spontaneous hydration. The experiment was done in triplicate.

162 **2.7. Protein electrophoresis and activity-gel analysis**

163 Crude protein profiles were examined by SDS–PAGE using 12% resolving and 4% stacking gels
164 following Laemmli *(22)*, and the separated bands were visualised with Coomassie Brilliant Blue R-
165 250. Carbonic anhydrase activity in the 10–100 kDa protein fraction was assessed by native PAGE
166 protonography using bromothymol blue and chilled CO_2-saturated water, with bovine carbonic
167 anhydrase as the positive control *(16, 23)*. Urease activity was similarly evaluated by native
168 zymography in phosphate buffer containing urea and phenol red, using jack-bean urease as the
169 positive control. Enzyme activity was indicated by visible colour changes in the corresponding bands.

170 **2.8. Optimization of growth and enzyme production**

171 Three sets of parallel cultures, MS1, LS1 and SED, were tested. LB broth was aliquoted into 4 mL
172 volumes, and a 2% (v/v) aliquot of a 24 h starter culture was added to each culture (except for the
173 variation of a factor). The tested factors were temperature ranging from 20 to 55 °C with an interval
174 of 5 units, initial pH (5–11), NaCl (0, 2, 4, 6 and 8% w/v in modified LB without basal NaCl), medium
175 type (LB, nutrient broth, urea broth, Zobell marine broth and tryptic soy broth), KCl (0, 2, 4, 6, 8 and
176 10 mM), inoculum size (0.5, 1.0, 1.5, 2.0 and 2.5% v/v) and $FeSO_4$ (0, 2, 4, 6, 8 and 10 mM). After
177 48 h, bacterial growth was measured by OD_{600}, and associated esterase and urease activity was
178 measured using the above assays. The test was done in triplicate.

179 **2.9. Biofilm quantification during mineralization**

180 The crystal violet microtiter plate method was used to estimate the formation of biofilm. The wells
181 were filled with LB broth prepared in CA and the urease pathway as described in the next section. A
182 sample in each pathway was taken (230 µL), and 20 µL of a 1:10 diluted overnight culture was
183 incubated at 37 °C for 24 hours, then washed three times with phosphate-buffered saline, fixed with
184 methanol for 15 minutes, stained with 1% crystal violet for 5 minutes, and washed. Bound dye was
185 solubilized by adding 33% acetic acid, and OD was measured at 570 nm. The strength of the biofilm

was determined based on the ODc (optical-density cut-off) of the negative control as described by Stepanović *et al*. *(24)*.

2.10. $CaCO_3$ precipitation and recovery

Qualitative mineralization was carried out on LB medium containing 0.75% (*w/v*) $CaCl_2$ and 2% (*w/v*) urea at 36 °C for 48 h. Using stereomicroscopy (40×), crystals were examined. For quantitative assessment of $CaCO_3$ precipitation through the urease pathway, cultures were grown in LB broth supplemented with filter-sterilized 0.75% (*w/v*) $CaCl_2$, 2% (*w/v*) urea, and 10 µM $NiCl_2$. For carbonic anhydrase-mediated precipitation, LB broth was supplemented with 0.75% (w/v) $CaCl_2$, 10 µM $ZnSO_4$, and 25 mM $NaHCO_3$. The precipitates were collected, washed thrice with distilled water, filtered, and dried at 70 °C until constant weight. Mineral yield was calculated as dry mineral per litre of culture. Both formulations were tested separately *(13, 25)*.

2.11. 16S rRNA gene amplification and phylogenetic analysis

Genomic DNA was extracted from isolates MS1, LS1, and SED using the HiPurA® Bacterial Genomic DNA Purification Kit (HiMedia Laboratories Pvt. Ltd., India; Cat. No. MB505-20PR), following the manufacturer's instructions. The 16S rRNA gene was amplified using universal bacterial primers 27F and 1492R *(26)***.** PCR products were resolved on a 0.8% agarose gel, purified, and subjected to Sanger sequencing. Forward and reverse reads were edited and assembled in BioEdit *(27)*, and the consensus sequences were compared with sequences in NCBI GenBank using BLASTn *(28)*. The isolate sequences and selected reference sequences were aligned using ClustalW *(29)***.**

Phylogenetic trees were reconstructed using maximum likelihood in MEGA12 *(30)*, with the Tamura three-parameter substitution model *(31)*. Variation in evolutionary rates among sites was modelled using a discrete gamma distribution with five categories (T92+G). Initial trees for the heuristic search were generated using neighbour joining *(32).* Alignment positions with less than 90% site coverage were excluded using partial deletion, and branch support was assessed using 1,000 bootstrap

replicates *(33)*. Isolates were assigned to the genus level when the 16S rRNA sequences did not clearly distinguish closely related species *(34)*.

2.12. Characterization of biomineralized material

Dried precipitates were mounted on aluminum stubs, gold-coated using a JEOL JFC-1600 fine coater, and examined with a JEOL JSM-6390LA scanning electron microscope equipped with an Oxford X-MaxN EDX detector. SEM imaging and EDX analysis were performed under high vacuum at an accelerating voltage of 15 kV and a working distance of approximately 10 mm. EDX spectra were acquired for 60 seconds from representative areas. Conductive coating and SEM–EDX analysis are consistent with approaches used recently to characterize microbially precipitated $CaCO_3$ *(35, 36)*.

Powder X-ray diffraction was performed on a Bruker D8 Advance diffractometer using Cu Kα radiation (λ = 1.54060 Å) in coupled 2θ/θ continuous-scan mode at 40 kV and 35 mA. Diffraction patterns were collected from 10.000° to 80.005° 2θ with a step size of 0.020°, a scan rate of approximately 4° min^{-1}, and a sample rotation rate of 15 rpm. Crystalline phases were assigned by comparison with ICDD PDF-2 and ICSD reference data using TOPAS 6. The XRD was used for phase identification, whereas SEM and EDX were used to assess morphology and elemental composition, respectively *(35)*.

2.13. Identification of carbonic anhydrase and urease genes

The carbonic anhydrase and urease genes were mined from the whole-genome sequence of MS1, LS1, and SED available in NCBI (Paul *et al*., Paper communicated; BioProject No. SNP260377). Annotated genomes were screened for CA- and urease-related genes. Candidate coding sequences were evaluated using BLASTX/BLASTP *(28)*, the NCBI Conserved Domain Database *(37)*, and InterPro *(38)*. Selected amino-acid sequences were submitted to AlphaFold for three-dimensional structure prediction *(39)* and visualized in UCSF ChimeraX *(40)*. Structural predictions were used as supporting evidence for protein annotation only and were not interpreted as proof of transcription, translation, or enzyme activity.

2.14. Statistical analysis

All analyses used the raw triplicate measurements, and data are reported as mean ± standard deviation (SD). For each experimental factor and response, a separate two-way fixed-effects analysis of variance (ANOVA) was fitted with condition, isolate, and the condition × isolate interaction as fixed effects *(41, 42, 43)*:

$$Y_{ijk} = \mu + C_i + S_j + (C \times S)_{ij} + \varepsilon_{ijk}$$

where Y_{ijk} is the observed response, μ is the overall mean, C_i is the effect of condition i, S_j is the effect of isolate j, $(C \times S)_{ij}$ is the interaction, and ε_{ijk} is residual variation among parallel culture tubes. Partial eta-squared (ηp^2) was reported for factorial models, and eta-squared (η^2) for strain-specific one-way ANOVA models *(44)*. Pairwise comparisons were performed using Tukey's honest significant difference procedure (*45)*.

Residual normality and homogeneity of variance were assessed using the Shapiro–Wilk test and the Brown–Forsythe modification of Levene's test, respectively *(46, 47)*. When residual normality was not achieved, rank-transformed factorial models were fitted as sensitivity analyses. Tests were two-sided at a nominal $\alpha = .05$. A Holm correction across the 63 omnibus effects was additionally used as a conservative familywise-error sensitivity analysis *(48)*. Analyses were performed in Python using SciPy and statsmodels *(49, 50)*.

3. Results

3.1. Isolation and screening of environmental isolates

A total of 50 bacterial isolates were recovered from the 11 different environmental samples, of which 19 were urease-positive. Urease-positive cultures changed phenol-red urea broth from yellow to pink. Preliminary CA-associated activity was indicated by yellow colonies on pNPA-supplemented nutrient agar and a deep-yellow response in the corresponding broth assay (Supplementary **Figs. 1**D and E). Sampling-site details, isolate distribution, and screening outcomes are provided in Supplementary Tables 1 and 2.

Growth was assessed at 0, 3, 5, and 7 mM pNPA. Concentrations above 3 mM reduced bacterial growth, whereas 3 mM produced a visible colony without visible growth inhibition (Supplementary **Figs. 1**A–C). MS1, LS1, and SED were selected for further analysis on the basis of their combined urease-positive and pNPA-screening responses.

3.2. Phenotypic and biochemical differentiation

The bacteria sample MS1, LS1, and SED formed creamy-white colonies with entire margins but differed in colony morphology. MS1 formed small, smooth colonies, LS1 formed medium-sized, slightly raised colonies, and SED formed large, mucoid colonies. All three isolates were Gram-positive, motile, endospore-forming, and positive in the urease and CA-associated screening assays. MS1 and LS1 were oxidase-positive, whereas SED was oxidase-negative. DNase activity was detected only in MS1; none of the isolates showed amylase or cyclodextrin glycosyltransferase activity (Supplementary Table 3).

3.3. Electrometric CO_2-hydration activity

Wilbur–Anderson CO_2-hydration activity differed among the isolates. SED showed the highest activity (44.40 ± 2.00 WAU mg^{-1}), followed by LS1 (26.58 ± 0.60 WAU mg^{-1}) and MS1 (23.76 ± 0.52 WAU mg^{-1}).

3.4. Protein profiling and activity-gel analysis

Denaturing SDS–PAGE of crude extracts from MS1, LS1, and SED showed complex protein profiles, with prominent bands at approximately 25–35 kDa and a major band around 63–66 kDa (**Fig.1**). The bovine CA control produced a strong band near its expected monomeric size. Protonography produced clear yellow activity zones for LS1 and SED, whereas the MS1 zone was faint and poorly defined. The bovine CA positive control produced distinct activity zones (**Fig. 1**). Protonographic migration positions were not used for molecular-mass assignment. Native urease zymography produced distinct pink activity bands for all three isolates. Bands were stronger for LS1 and MS1 and weaker for SED. The jack-bean urease positive control produced two activity zones. Native-gel migration positions were not used to estimate molecular mass (**Fig. 1**).

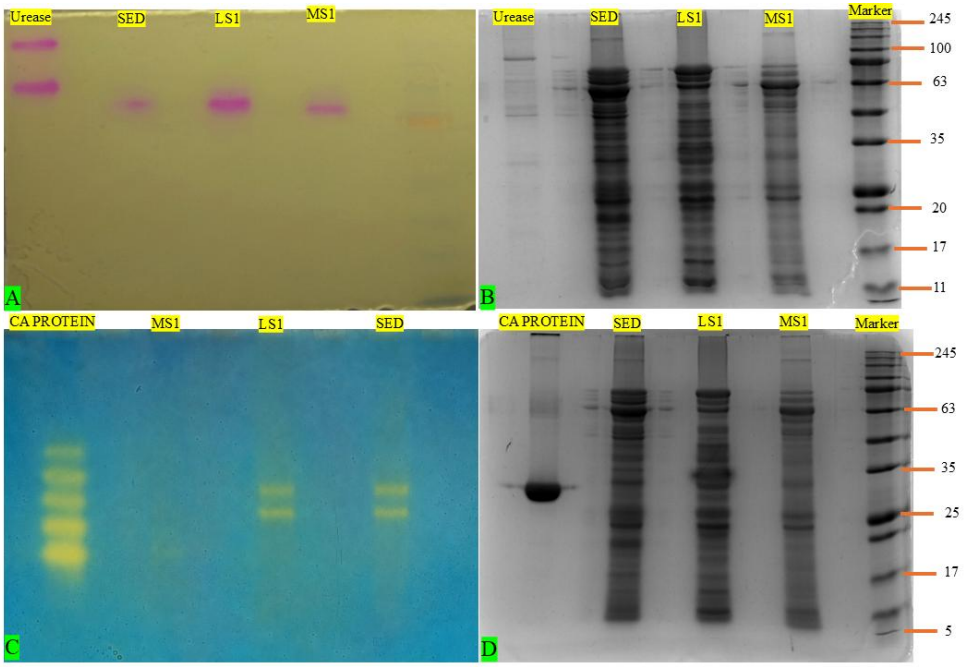


Fig.1 Protein profiles and activity-gel detection of urease and carbonic anhydrase (CA) in crude extracts of MS1, LS1, and SED. (A) Native urease zymography showing pink activity bands, with jack-bean urease as the positive control; (B) corresponding SDS–PAGE profiles; (C) CA protonography showing yellow activity zones, with bovine CA as the positive control; and (D) corresponding SDS–PAGE profiles. Molecular-mass markers are shown in kDa.

3.5. Enzyme activity under optimized production conditions

The enzymatic performance of the selected isolates was evaluated under the final optimized production conditions. Considerable variation was observed among isolates, indicating differences in their metabolic capacity for CO_2 hydration and urea hydrolysis. Among the tested isolates, SED exhibited the highest CA-associated activity (4.130 ± 0.458 U mL^{-1}), followed by LS1 (3.357 ± 0.192 U mL^{-1}) and MS1 (2.211 ± 0.349 U mL^{-1}). In contrast, LS1 showed the highest urease activity (31.289 ± 2.381 U mL^{-1}), while MS1 and SED exhibited relatively similar activities (22.319 ± 0.307 and 21.693 ± 1.753 U mL^{-1}, respectively). This has been tabulated and recorded in Table 1 in comparison with related work that has been published.

3.6. Effects of physicochemical and culture parameters on growth and enzyme activity

3.6.1. Temperature and pH

All three isolates showed maximum or near-maximum responses at 35 °C. MS1 showed the highest growth and CA-associated activity at this temperature, whereas LS1 showed the highest urease activity (**Fig. 2**). At 55 °C, mean growth, CA-associated activity, and urease activity were 97.6%, 97.4%, and 87.2% lower, respectively, than their corresponding maxima.

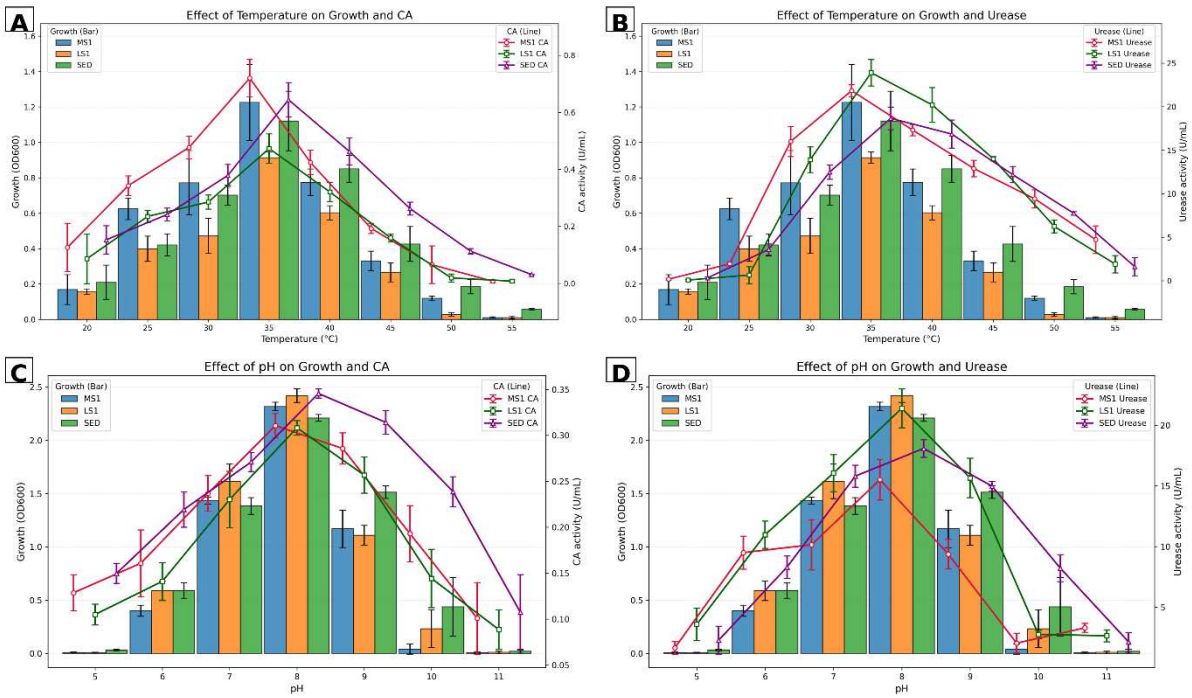


Fig. 2 Effects of temperature and pH on growth and enzyme activity of MS1, LS1, and SED. (A) Temperature-dependent growth and CA-associated activity; (B) temperature-dependent growth and urease activity; (C) pH-dependent growth and CA-associated activity; and (D) pH-dependent growth and urease activity. Error bars indicate standard deviations.

The optimum pH for all three isolates was pH 8. LS1 showed the highest growth and urease activity, whereas SED showed the highest CA-associated activity (**Fig. 2**). From pH 8 to 11, mean growth, CA-associated activity, and urease activity decreased by 99.5%, 69.2%, and 85.3%, respectively.

3.6.2. NaCl concentration and growth medium

Growth, CA-associated activity, and urease activity were highest or near-highest at 2% (*w/v*) NaCl. At this concentration, LS1 showed the highest growth and urease activity, whereas SED showed the

highest CA-associated activity (**Fig. 3**). At 8% NaCl, mean growth, CA-associated activity, and urease activity were 97.3%, 88.8%, and 95.0% lower, respectively, than their corresponding maxima. LB medium produced the highest overall responses among the tested media, whereas tryptic soy broth produced the lowest or near-lowest responses. In LB medium, LS1 showed the highest growth and urease activity, and SED showed the highest CA-associated activity (**Fig. 3**).

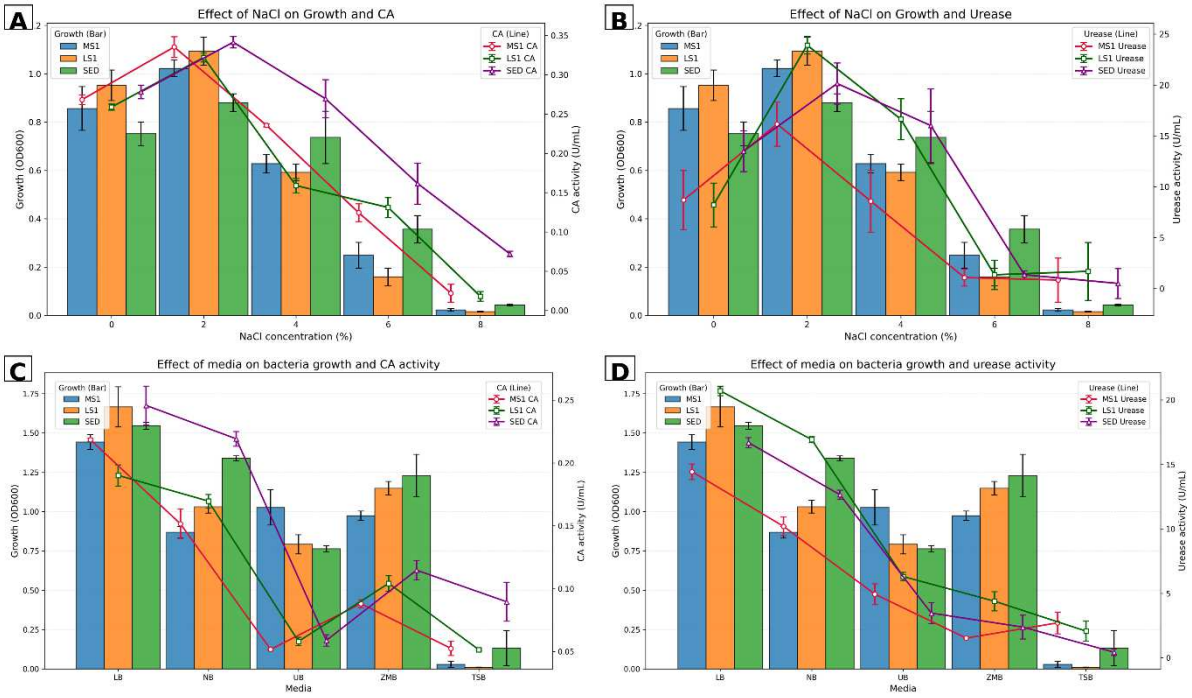


Fig. 3 Effects of NaCl concentration and growth medium on growth and enzyme activity of MS1, LS1, and SED. (A) NaCl-dependent growth and CA-associated activity; (B) NaCl-dependent growth and urease activity; (C) growth-medium effects on growth and CA-associated activity; and (D) growth-medium effects on growth and urease activity. NaCl is expressed as % (w/v); error bars indicate standard deviations.

3.6.3. Potassium, Iron metal salts, and inoculum size

Monovalent KCl salt produced smaller variations. Maximum overall responses occurred at approximately 4 mM KCl; at this concentration, MS1 showed the highest growth and CA-associated activity, whereas LS1 showed the highest urease activity. At 10 mM KCl, the overall mean responses were 19.2–20.7% below their corresponding maxima (Supplementary **Fig. 2**A and B). With the iron metal salt ($FeSO_4$), maximum bacterial growth occurred without added $FeSO_4$. CA-associated

activity reached maximum at 4 mM, and urease activity was highest at 2 mM. At 10 mM $FeSO_4$, mean growth, CA-associated activity, and urease activity were lower by 76.3%, 76.9%, and 91.3%, respectively, than their corresponding maxima. The increase in CA-associated activity at 4 mM was not consistent relative to the $FeSO_4$-free condition within individual isolates (Supplementary **Fig. 2**C and D). An inoculum size of 2% generally produced the highest growth, CA-associated activity, and urease activity, except for MS1 growth, which was highest at 1.5%. At the optimum inoculum level, SED showed the greatest response for all three measured parameters. Increasing the inoculum to 2.5% reduced overall mean responses by 6.2–10.1% (Supplementary **Fig. 2** E and F).

3.7. Genomic detection of biomineralization-related genes and predicted protein structures

Genome analysis identified β-class carbonic anhydrase and urease α-subunit (UreC) genes in MS1, LS1, and SED derived from the whole genome of these isolates (BioProject No. SNP260377, Paul *et al*., Paper under communication). In MS1, the predicted β-class carbonic anhydrase gene MLGHON_03835 encoded a protein of 188 amino acids, while the UreC gene MLGHON_02084 encoded a protein of 571 amino acids (**Fig. 4**). In LS1, BCMDIH_04725 and BCMDIH_03527 encoded the corresponding proteins of 187 and 590 amino acids, respectively. In SED, JPCGHI_04088 was annotated as β-class carbonic anhydrase and JPCGHI_02158 as UreC, with both proteins reported to be 187 amino acids long (**Fig. 4**).

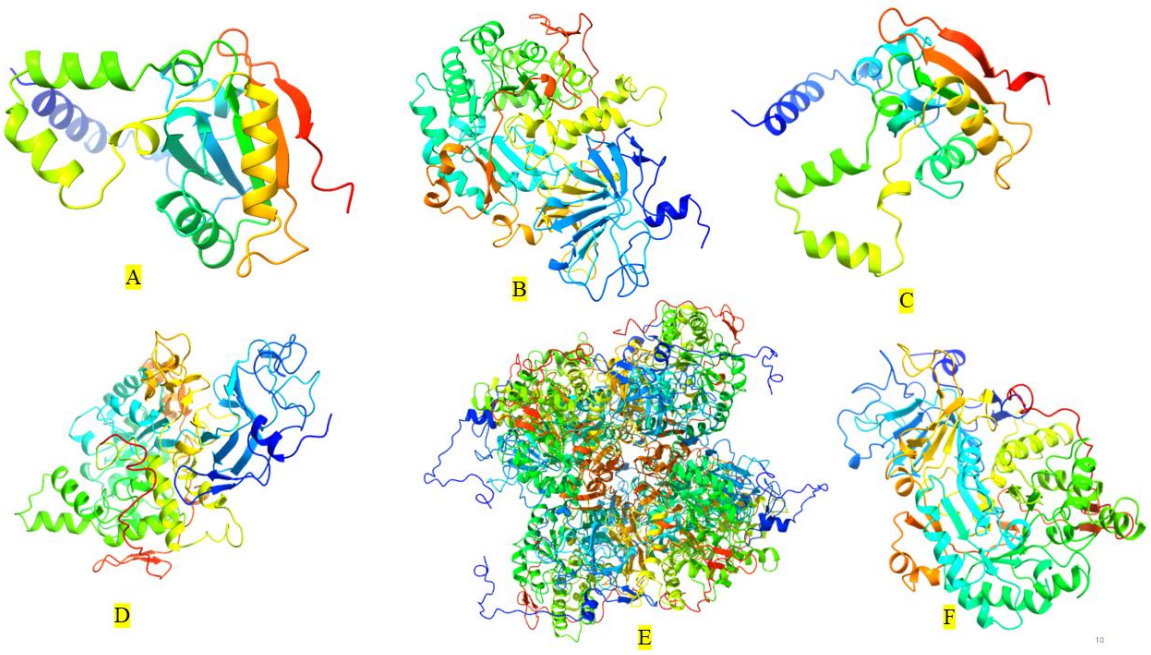


Fig. 4 Predicted three-dimensional structures of β-class carbonic anhydrase and UreC proteins from MS1, LS1, and SED. Panels A–C show β-class carbonic anhydrases MLGHON_03835, BCMDIH_04725, and JPCGHI_04088, respectively; panels D–F show the corresponding UreC proteins MLGHON_02084, BCMDIH_03527, and JPCGHI_02158. Ribbon models show the predicted overall folds and structural organization.

3.8. Statistical analysis

Condition was significant in all 21 single-factor models (all $p < .001$), with large partial effect sizes ($\eta p^2 = .588–.995$) for bacterial growth, CA-associated activity, and urease activity. The isolate main effect was significant in 19 of 21 models; NaCl-dependent growth and $FeSO_4$-dependent CA-associated activity were the exceptions. Eighteen conditions × isolate interactions were significant at the nominal $\alpha = .05$ level, and 16 remained significant after Holm correction. The temperature × isolate interaction for growth, and the $FeSO_4$ × isolate interaction for CA-associated activity were not significant after global Holm correction. Rank-transformed sensitivity analyses reproduced the nominal significance pattern for the four models with non-normal residuals (Supplementary Table 4).

3.9. Biomineralization and mineralogical characterization

3.9.1. Crystallization, biofilm formation, and $CaCO_3$ production

Stereo light microscopy showed distinct colony-associated mineral deposition patterns. MS1 produced dense, compact aggregates, LS1 formed clustered semi-compact deposits, and SED produced predominantly peripheral, ring-like deposits (**Figs. 5**A–C).

SED showed the greatest crystal violet biofilm biomass and was classified as a strong biofilm former, whereas MS1 and LS1 showed moderate biofilm-forming capacity. SED produced the lowest $CaCO_3$ yield in both the CA-associated and urease-mediated assays. MS1 produced the highest mineral yield under CA-associated conditions, while MS1 and LS1 produced the greatest yields under urease-mediated conditions (**Figs. 5**D–E).

Urease-mediated precipitation produced greater $CaCO_3$ yields than the CA-associated assay, particularly for MS1 and LS1. Abiotic controls produced only trace precipitates.

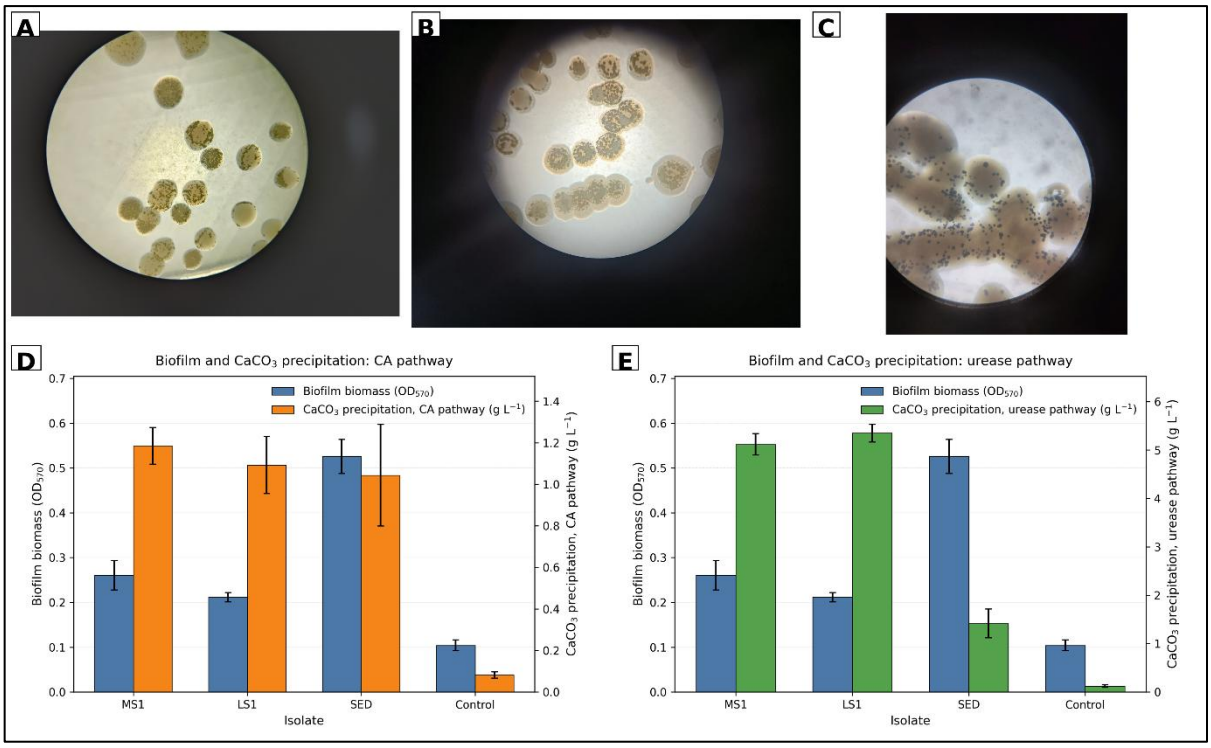


Fig. 5 Isolate-dependent $CaCO_3$ crystallization, biofilm formation, and mineral production by MS1, LS1, and SED. Stereomicrographs at 40× magnification show colony-associated mineral deposits produced by (A) MS1, (B) LS1, and (C) SED. Biofilm biomass and $CaCO_3$ yield are shown for (D)

CA-associated and (E) urease-mediated precipitation assays, including abiotic controls. Error bars indicate replicate variability.

3.9.2. Mineral morphology and elemental composition

SEM imaging showed isolate-specific mineral morphologies (**Figs. 6**A–C). MS1 formed irregular to sub-spherical particles with rough surfaces and extensive agglomeration. LS1 produced a heterogeneous assemblage of granular and plate-like particles with comparatively well-defined edges. SED formed compact mineral aggregates in the examined regions.

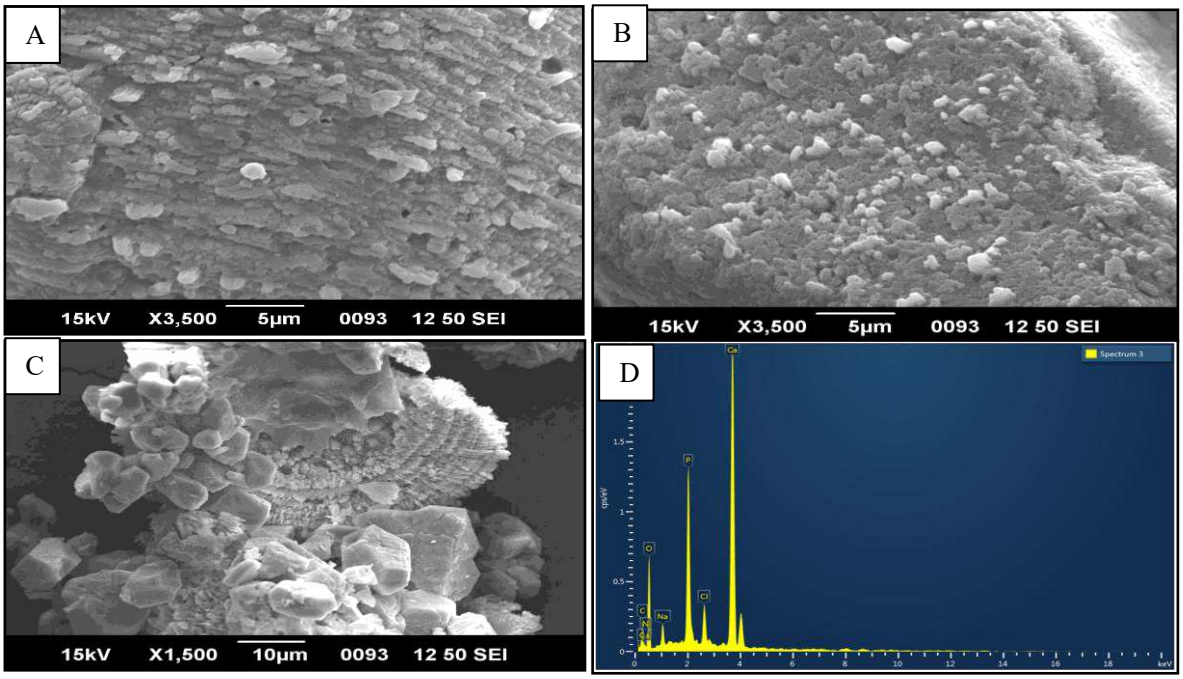


Fig. 6 Morphology and elemental composition of bacterially precipitated calcium carbonate. Representative SEM micrographs of precipitates produced by (A) MS1, (B) LS1, and (C) SED; (D) representative EDX spectrum showing dominant Ca, C, and O signals with minor P, Na, and Cl.

3.9.3. Crystalline phases

X-ray diffraction patterns from MS1, LS1, and SED contained reflections assigned to calcite, vaterite, and aragonite (**Figs. 7**A–C). Calcite produced the most prominent peak in each pattern, while the relative intensities of vaterite- and aragonite-associated peaks varied among the isolates.

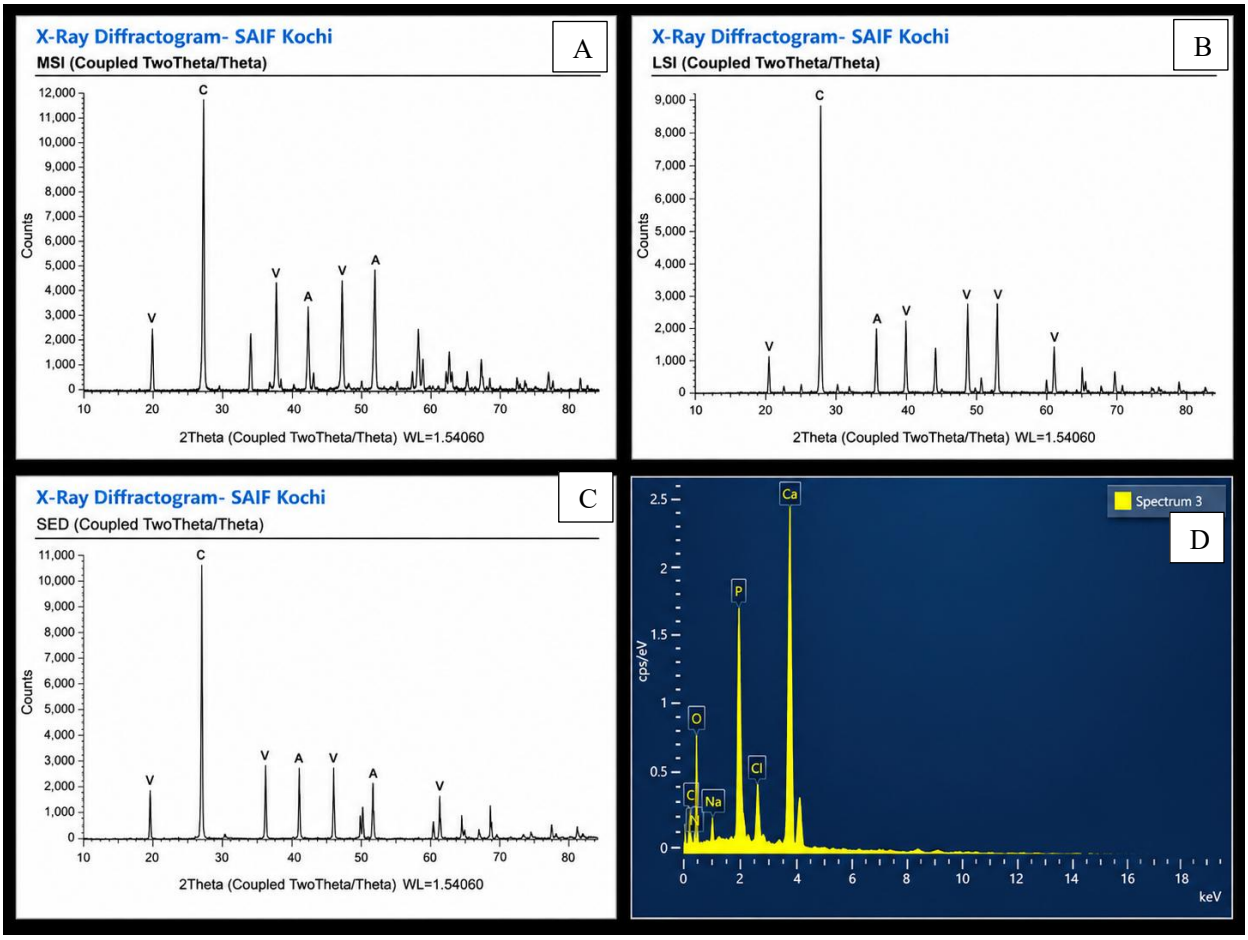


Fig. 7 X-ray diffraction (XRD) patterns of bacterial $CaCO_3$ precipitates produced by (A) MS1, (B) LS1, and (C) SED, with (D) energy-dispersive X-ray spectroscopy (EDX) data showing their elemental composition. Diffraction peaks assigned to calcite (C), vaterite (V), and aragonite (A) are labelled.

3.10. Molecular identification by 16S rRNA gene analysis

Amplification of the 16S rRNA gene from MS1, LS1, and SED yielded products of approximately 1.5 kb (**Fig. 8**A), with sequence lengths of 1,421, 1,420, and 1,410 bp, respectively. Phylogenetic analysis placed MS1 and LS1 within *Lysinibacillus* and SED within *Bacillus*. MS1 grouped with the *L. macroides–L. pakistanensis* lineage, although bootstrap support was low (29%; **Fig. 8**B). LS1 clustered with *L. fusiformis* (73% support; **Fig. 8**D), whereas SED clustered with *B. cereus* (52% support; **Fig. 8**C). Given the limited species-level resolution, the isolates were designated

Lysinibacillus sp. MS1, *Lysinibacillus sp*. LS1, and *Bacillus sp*. SED. Their 16S rRNA gene sequences were submitted to NCBI GenBank under accession numbers QB160454 (LS1), QB160455 (MS1), and QB160456 (SED).

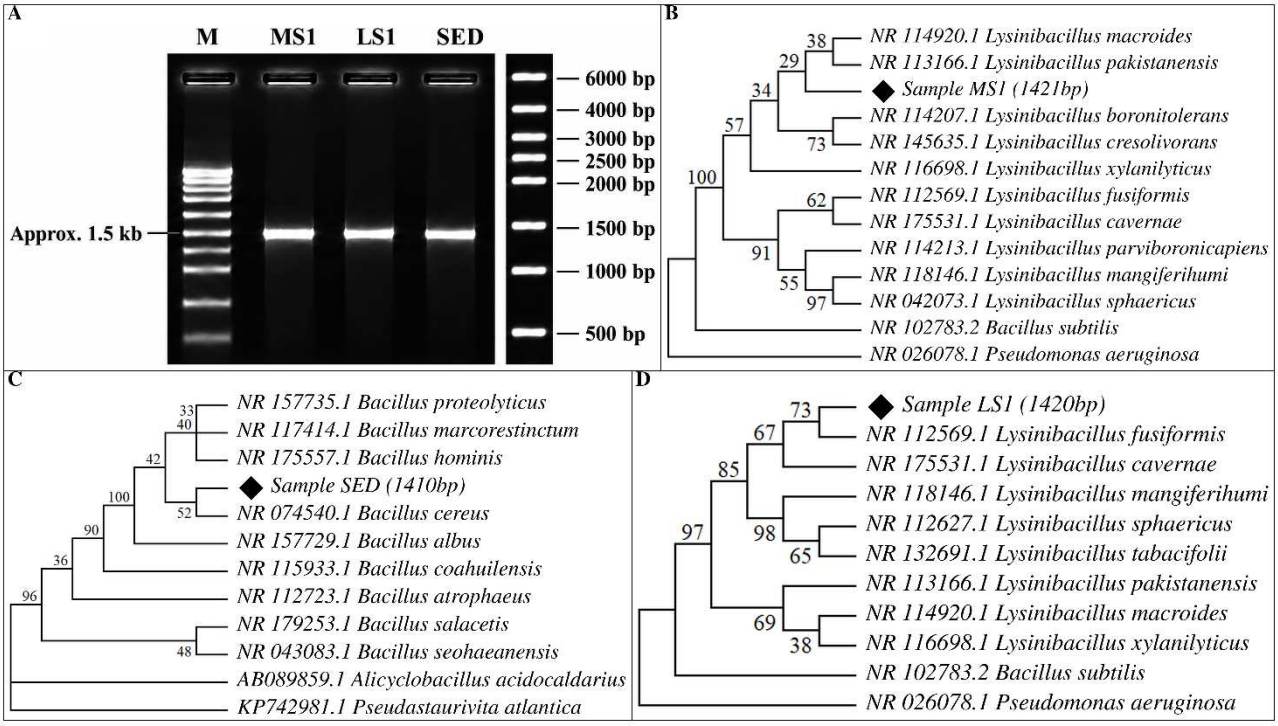


Fig. 8 16S rRNA gene-based identification of bacterial isolates. (A) PCR products of MS1, LS1, and SED showing bands at approximately 1.5 kb; M denotes the DNA size marker. Phylogenetic trees show the placement of (B) MS1, (C) SED, and (D) LS1 relative to reference sequences. Black diamonds indicate the study isolates, and numbers at the nodes represent bootstrap support (%).

4. Discussion

4.1. Evidence for dual urease and carbonic anhydrase activity

Evidence for dual enzymatic capacity came from several independent levels of analysis. The screening assays and quantitative measurements detected both urease and CA-associated activity in MS1, LS1, and SED; activity gels provided a second experimental readout; and genome annotation identified genes consistent with both functions. Biochemically, the two routes are distinct: urease promotes alkalinization through urea hydrolysis, whereas CA accelerates the reversible hydration of

CO_2 to bicarbonate. Their co-occurrence has been described in carbonate-precipitating bacteria and has recently been used to identify strains with broader biomineralization potential *(25, 36, 51)*.

The more informative result, however, was that the three isolates did not rank in the same order across assays. SED had the highest CO_2-hydration and CA-associated activities, LS1 had the highest urease activity, and MS1, despite intermediate enzyme activities, produced the greatest mineral yield in the CA-associated precipitation assay. The isolates are therefore, better viewed as complementary phenotypes than as a single hierarchy of performance. Strain-dependent differences of this kind are increasingly evident in both ureolytic and CA-associated biomineralization systems *(12, 36, 52)*.

The CA-associated measurements also require careful interpretation. pNPA hydrolysis is a useful screening for CA esterase activity, but crude extracts can contain unrelated esterases that act on the same substrate. For that reason, the pNPA result was not treated as stand-alone proof of CA. It was considered alongside direct CO_2-hydration measurements, protonography, and predicted CA genes. Likewise, protonographic migration was not used to infer molecular mass because band position can be altered by conformation, oligomeric state, renaturation, and proton diffusion *(15, 16, 53)*. Numerical comparisons among published enzyme activities should be made cautiously because preparation methods, substrates, assay conditions, and units differ. Selected literature values are summarized in Table 1.

Table 1. Reported carbonic anhydrase- and urease-associated activities in selected biomineralization studies and the present isolates. Values are reproduced as reported in the cited studies; direct numerical comparison is limited by differences in assay design, enzyme preparation, substrates, and activity units.

Enzyme	**Isolate**	**Reported activity**	**Assay or preparation**	**Context**	**Ref.**
Carbonic anhydrase	*Bacillus licheniformis*	2.31 U mL^{-1}	Crude enzyme; pNPA hydrolysis	CA-associated esterase assay	*(61)*
Carbonic anhydrase	*Bacillus licheniformis* U-1	1.39 U mL^{-1}	pNPA hydrolysis	Biocementation study	*(12)*
Carbonic anhydrase	*Bacillus pumilus* U-21	1.50 U mL^{-1}	pNPA hydrolysis	Soil-derived CA-associated isolate	*(12)*

Enzyme	Isolate	Reported activity	Assay or preparation	Context	Ref.
Carbonic anhydrase	*Aeromonas hydrophila*	2.10 EU mL^{-1}	Intracellular crude extract; CO_2-hydration assay	Freshwater CA-producing isolate	*(62)*
Carbonic anhydrase	*Enterobacter taylorae*	3.86 EU mL^{-1}	Intracellular crude extract; CO_2-hydration assay	CA-producing isolate	*(62)*
Carbonic anhydrase	MS1	2.211 ± 0.349 U mL^{-1}	Optimized crude-enzyme assay	CA-associated esterase activity	Present study
Carbonic anhydrase	LS1	3.357 ± 0.192 U mL^{-1}	Optimized crude-enzyme assay	CA-associated esterase activity	Present study
Carbonic anhydrase	SED	4.130 ± 0.458 U mL^{-1}	Optimized crude-enzyme assay	CA-associated esterase activity	Present study
Urease	*Sporosarcina pasteurii*	13.6 ± 0.3 U mL^{-1}	Cell-free supernatant assay	MICP reference organism	*(63)*
Urease	*Bacillus halodurans* PO15	28.0 U mL^{-1}	Pre-optimization culture	Mangrove isolate	*(54)*
Urease	*Citrobacter freundii* Y2b	45.4 ± 3.4 U mL^{-1}	Cell-free supernatant assay	Environmental isolate	*(63)*
Urease	*Bacillus thuringiensis* Y3a	45.0 ± 7.3 U mL^{-1}	Cell-free supernatant assay	Urease-producing isolate	*(63)*
Urease	*Pseudomonas azotoformans* C	54.9 ± 3.5 U mL^{-1}	Cell-free supernatant assay	Environmental isolate	*(63)*
Urease	SED	21.693 ± 1.753 U mL^{-1}	Optimized production assay	Urease activity	Present study
Urease	MS1	22.319 ± 0.307 U mL^{-1}	Optimized production assay	Urease activity	Present study
Urease	LS1	31.289 ± 2.381 U mL^{-1}	Optimized production assay	Urease activity	Present study

4.2. Environmental control of growth and enzyme activity

Temperature and pH have influenced shifts in growth and enzyme activity. All three isolates performed best around 35 °C and pH 8, conditions that fall within the mesophilic, mildly alkaline range commonly associated with effective microbial carbonate precipitation *(1, 3)*. The sharp decline at 55 °C and at strongly alkaline pH was recorded, indicating that higher temperature or alkalinity does not increase biomineralization capacity once the physiological tolerance of the cells is exceeded.

A similar pattern was evident for salinity. Responses peaked or remained near their maxima at 2% NaCl but fell markedly at 8% NaCl. Recent work in coastal carbonate-forming bacteria also showed that salinity effects on CA activity and mineral formation depend strongly on strain and medium

composition *(52)*. LB media supported the highest overall responses in the present study, whereas tryptic soy broth was the least favorable media, consistently. Culture composition, therefore, mattered alongside temperature, pH, and salinity; this agrees with optimization studies showing that urease production in *Bacillus* can vary substantially with growth conditions *(54)*.

Monovalent KCl salt caused comparatively modest changes, whereas high $FeSO_4$ salt concentrations strongly suppressed growth and both enzyme-associated responses. A 2% inoculum generally gave the highest responses, with only a small decline at 2.5%. The statistical analysis strengthens these observations: condition effects were large across all models, and most condition × isolate interactions remained significant after multiplicity correction. A single set of culture conditions can therefore provide a useful starting point, but the response magnitude remains strain-specific.

4.3. Genomic support and predicted protein structures

Genome annotation was consistent with the biochemical activities observed in the three isolates. Each genome contained putative β- and γ-class CA candidates together with urease structural and accessory genes, although the UreB assignment in SED remains putative. UreC encodes the catalytic α-subunit, but *ureC* alone does not establish the capacity to produce a mature, active urease complex. The accompanying accessory genes therefore strengthen the genomic support for urease function. Hoffmann *et al*. *(55)* demonstrated that urease gene expression and associated transport functions can influence ureolytic activity and calcite precipitation, with their effects depending on culture conditions.

The strain LS1 showed the highest measured urease activity and urease-mediated mineral yield, while MS1 produced a numerically similar mineral yield and shared a highly conserved UreC sequence with LS1. In contrast, isolate SED combined the broadest CA-annotated repertoire with the highest CA-associated esterase and CO_2-hydration activities. This makes its additional CA candidates relevant targets for functional investigation, but it does not necessarily indicate that gene number determines activity. Neither the Y97H sequence difference nor the short, 71-amino-acid CA-annotated product can yet be assigned a role in this phenotype. Sharma *et al*. *(56)* similarly examined

genome annotations alongside CA and urease activities and carbonate precipitation in *Bacillus paranthracis* CT5, providing a precedent for interpreting these forms of evidence together.

The activity and mineral-yield rankings also differed: MS1 produced the highest CA-associated mineral yield despite SED having the highest measured CA activities. Enzyme activity under the production conditions therefore did not directly predict mineral recovery in the separate precipitation assays. Cappa *et al. (14)* used labelled urea to examine the carbon source of precipitated carbonate in *Bacillus megaterium* and found that CO_2 availability affected the relative contribution of the mineralization pathways. Zhu *et al. (57)* identified CA- and urease-associated genes in *Brevibacterium linens* BS258 and linked increased CA expression with calcite dissolution under the conditions examined. These findings underline the importance of interpreting CA-related genomic potential in the context of the mineralization conditions.

Protein-structure predictions can extend sequence-based annotation when model quality, sequence coverage, and relevant functional features are assessed. A plausible predicted fold, however, does not demonstrate transcription, protein production, assembly, or catalytic activity. Ma *et al. (58)* strengthened the link between genome-derived urease sequences and mineralization in *Neobacillus mesonae* NS-6 by combining structural modelling with targeted mutations and biochemical measurements. For the present isolates, identifying individual candidate proteins would require evidence such as proteomic identification and establishing their contribution to activity or mineralization would require targeted functional testing, for example, gene disruption and complementation or purified-enzyme assays.

The biochemical assays and activity gels provide functional support at the isolate level, while microscopy, SEM–EDX and XRD document the resulting minerals. Together with the genomic findings, they support complementary CA- and urease-associated capabilities. They do not identify which CA candidate produced the measured activity or assign calcite, vaterite, or aragonite formation to a particular protein. Because the two mineralization pathways were tested separately, their

coexistence in these isolates should be interpreted as dual capability rather than demonstrated synergy.

4.4. Biomineralization efficiency, biofilm formation, and pathway specificity

Urease-mediated precipitation generated considerably more $CaCO_3$ than the CA-associated assay for MS1 and LS1. Rapid alkalinization during urea hydrolysis offers a straightforward explanation for that difference, but the two assays were not chemically equivalent: they differed in substrate supply, carbonate flux, cofactors, and reaction environment. Mineral mass therefore cannot be used as a direct measure of the intrinsic efficiency of urease versus CA. The CA-associated system still produced substantially more precipitate than the abiotic control, consistent with reports of carbonate formation by native and engineered CA-producing bacteria *(12, 13)*. The carbon source itself can also shift pathway preference, as demonstrated by Cappa *et al*. *(14)*.

Isolate SED showed distinct biofilm formation and mineral yield. It produced the strongest crystal-violet signal but the lowest recovered $CaCO_3$ in both precipitation assays. Biofilms can promote nucleation by retaining cells, ions, enzymes, and negatively charged extracellular components, yet biomass alone does not determine how much mineral ultimately accumulates. Matrix composition, diffusion, local pH, calcium availability, and extracellular DNA can influence the location and growth of crystals *(4, 59)*. Biofilm biomass is therefore more informative for strain selection when considered alongside enzyme activity and mineral yield than when used as an individual predictor.

The study shows that each isolate can support precipitation in both urease-mediated and CA-associated systems, but the systems were tested separately. Therefore, no conclusion can be drawn about whether the two pathways act additively, synergistically, or antagonistically when they operate together. Earlier work proposed a synergistic role for urease and CA in carbonate mineralization *(25)*, while more recent dual-enzyme screening studies underscore the practical interest in this combination *(36)*. A direct test in MS1, LS1, and SED would require matched urease-only, CA-only, combined-pathway, and abiotic treatments under the same chemical conditions.

4.5. Mineralogy and taxonomic context

The microscopy, SEM–EDX, and XRD results describe different aspects of the same mineralization process. Microscopy and SEM documented isolate-dependent deposit morphology, EDX showed Ca, C, and O as the dominant elements in the recovered material, and XRD provided the phase-level evidence for calcite, vaterite, and aragonite. Multiple $CaCO_3$ polymorphs are common in microbial mineralization and can be influenced by supersaturation, ionic composition, precipitation kinetics, and interactions with cells or extracellular organic matter *(4, 5, 35)*. Calcite was the dominant crystalline phase in all three samples, while differences in the relative vaterite and aragonite-associated peak intensities point to isolate-specific mineralization environments.

Partial 16S rRNA phylogeny placed MS1 and LS1 within *Lysinibacillus* spp. and SED within *Bacillus* sp., in agreement with their Gram-positive, motile, endospore-forming phenotypes. The sequences clustered close to species complexes that are difficult to resolve with partial 16S rRNA gene alone, so genus-level assignment is the more defensible interpretation. From an applied perspective, spore-forming *Bacillales* are attractive because spores may improve handling and storage stability; however, recovery of metabolic and mineralization activity after storage must be established experimentally for each strain and formulation *(60)*.

4.6. Limitations and future directions

Several limitations constrain the present conclusions. The pNPA assay is not specific for CA in crude extracts; enzyme identities were not confirmed by purified-protein kinetics or targeted proteomics; genomic detection did not establish expression; partial 16S rRNA gene sequences limited species-level resolution; and XRD phase identification was qualitative rather than quantitative. Most importantly, urease- and CA-associated mineralization were evaluated in separate formulations. The data therefore demonstrate dual functional capacity, not an interaction between the two pathways.

The next experiments should place urease-only, CA-only, combined-pathway, and abiotic treatments under matched chemical conditions and follow pH, dissolved inorganic carbon, calcium, ammonia, and mineral production over time. Quantitative phase analysis and carbon-source tracing would

clarify how each pathway contributes to the final precipitate. Genome-based taxonomic analysis and targeted expression studies would strengthen strain identification and enzyme attribution. Finally, the most promising isolates should be tested in soil, sand, and cementitious matrices, with attention to strength improvement, permeability reduction, mineral durability, storage stability, ammonia release, and net carbon balance before application-scale claims are made.

5. Conclusions

This study demonstrated that LS1, MS1, and SED exhibit carbonic anhydrase (CA)-associated and urease activities and precipitate $CaCO_3$ in independently tested mineralization systems. Analysis of 16S rRNA gene sequences assigned LS1 and MS1 to the genus *Lysinibacillus* spp. and SED to *Bacillus* sp. Single-factor experiments indicated favourable conditions around pH 8, 2% NaCl, 4 mM KCl and a 2% inoculum in LB medium, providing a basis for further optimization.

The isolates displayed distinct functional strengths. Sample LS1 showed the highest urease activity and urease-mediated mineral yield, although MS1 produced a numerically similar yield. MS1 achieved the highest CA-associated mineral yield, whereas SED exhibited the highest CA-associated esterase activity, CO_2-hydration activity, and biofilm biomass. Genome annotation identified CA-related genes and urease structural and accessory genes in all three isolates, supporting their biochemical potential without establishing the contributions of individual candidate proteins. Microscopy and SEM characterized mineral morphology, EDX supported elemental characterization, and XRD identified calcite, vaterite, and aragonite among the precipitates.

The principal finding is that greater enzyme activity or biofilm biomass did not consistently correspond to greater mineral recovery. These traits are therefore informative but insufficient on their own for selecting effective biomineralizing strains. Selection should prioritize directly measured precipitation performance under the intended operating conditions, supported by biochemical and genomic characterization. The contrasting profiles of LS1, MS1, and SED offer complementary capabilities, while the separate mineralization experiments establish potential through both pathways without demonstrating synergy. Further work should evaluate the pathways together, experimentally

validate candidate gene functions, and determine whether laboratory performance is sustained in soil and cementitious materials. Establishing these links will provide a stronger basis for matching individual strains to specific biomineralization applications.

References

1. Castro-Alonso, M. J., Montañez-Hernandez, L. E., Sanchez-Muñoz, M. A., Macias Franco, M. R., Narayanasamy, R., and Balagurusamy, N. (2019) Microbially induced calcium carbonate precipitation (MICP) and its potential in bioconcrete: Microbiological and molecular concepts. Front. Mater., 6, 126. https://doi.org/10.3389/fmats.2019.00126

2. Dhami, N. K., Reddy, M. S., and Mukherjee, A. (2013) Biomineralization of calcium carbonates and their engineered applications: A review. Front. Microbiol., 4, 314. https://doi.org/10.3389/fmicb.2013.00314

3. Liu, Y., Ali, A., Su, J.-F., Li, K., Hu, R.-Z., and Wang, Z. (2023) Microbial-induced calcium carbonate precipitation: Influencing factors, nucleation pathways, and application in waste water remediation. Sci. Total Environ., 860, 160439. https://doi.org/10.1016/j.scitotenv.2022.160439

4. Zambare, N. M., Naser, N. Y., Gerlach, R., and Chang, C. B. (2020) Mineralogy of microbially induced calcium carbonate precipitates formed using single cell drop-based microfluidics. Sci. Rep., 10, 17535. https://doi.org/10.1038/s41598-020-73870-y

5. Zhuang, D., Yan, H., Tucker, M. E., Zhao, H., Han, Z., Zhao, Y., Sun, B., Li, D., Pan, J., Zhao, Y., Meng, R., Shan, G., Zhang, X., and Tang, R. (2018) Calcite precipitation induced by *Bacillus cereus* MRR2 cultured at different Ca^{2+} concentrations: Further insights into biotic and abiotic calcite. Chem. Geol., 500, 64–87. https://doi.org/10.1016/j.chemgeo.2018.09.018

6. Andrews, R. K., Blakeley, R. L., and Zerner, B. (1984) Urea and urease. Adv. Inorg. Biochem., 6, 245–283.

7. Konieczna, I., Żarnowiec, P., Kwinkowski, M., Kolesińska, B., Frączyk, J., Kamiński, Z. J., and Kaca, W. (2012) Bacterial urease and its role in long-lasting human diseases. Curr. Protein Pept. Sci., 13, 789–806. https://doi.org/10.2174/138920312804871094

8. Gadhvi, M. S., Javia, B. M., Vyas, S. J., Patel, R., and Dudhagara, D. R. (2024) *Bhargavaea beijingensis* a promising tool for bio-cementation, soil improvement, and mercury removal. Sci. Rep., 14, 23976. https://doi.org/10.1038/s41598-024-75019-7

9. Mwandira, W., Mavroulidou, M., Gunn, M. J., Purchase, D., Garelick, H., and Garelick, J. (2023) Concurrent carbon capture and biocementation through the carbonic anhydrase (CA) activity of microorganisms—a review and outlook. Environ. Process., 10, 56. https://doi.org/10.1007/s40710-023-00667-2

10. Boone, C. D., Habibzadegan, A., Gill, S., and McKenna, R. (2013) Carbonic anhydrases and their biotechnological applications. Biomolecules, 3, 553–562. https://doi.org/10.3390/biom3030553

11. Bose, H., and Satyanarayana, T. (2017) Microbial carbonic anhydrases in biomimetic carbon sequestration for mitigating global warming: Prospects and perspectives. Front. Microbiol., 8, 1615. https://doi.org/10.3389/fmicb.2017.01615

12. Mwandira, W., Mavroulidou, M., Timmermans, M., Gunn, M. J., Gray, C., Pantoja-Muñoz, L., and Purchase, D. (2024) A study of bacteria producing carbonic anhydrase enzyme for $CaCO_3$ precipitation and soil biocementation. Environ. Sci. Pollut. Res., 31, 45818–45833. https://doi.org/10.1007/s11356-024-34077-0

13. Gilmour, K. A., Sharma Ghimire, P., Wright, J., Haystead, J., Dade-Robertson, M., Zhang, M., and James, P. (2024) Microbially induced calcium carbonate precipitation through CO_2 sequestration via an engineered *Bacillus subtilis*. Microb. Cell Fact., 23, 168. https://doi.org/10.1186/s12934-024-02437-7

14. Cappa, M., Perego, C., Terzis, D., and Principi, P. (2025) *Bacillus megaterium* favours CO_2 mineralization into $CaCO_3$ over the ureolytic pathway. Sci. Rep., 15, 21861. https://doi.org/10.1038/s41598-025-07323-9

15. Pocker, Y., and Stone, J. T. (1967) The catalytic versatility of erythrocyte carbonic anhydrase. III. Kinetic studies of the enzyme-catalyzed hydrolysis of p-nitrophenyl acetate. Biochemistry, 6, 668–678. https://doi.org/10.1021/bi00855a005

16. De Luca, V., Del Prete, S., Supuran, C. T., and Capasso, C. (2015) Protonography, a new technique for the analysis of carbonic anhydrase activity. J. Enzyme Inhib. Med. Chem., 30, 277–282. https://doi.org/10.3109/14756366.2014.917085

17. Wei, H., Lunin, V. V., Alahuhta, M., Himmel, M. E., Huang, S., Bomble, Y. J., and Zhang, M. (2024) Streamlining heterologous expression of top carbonic anhydrases in *Escherichia coli*: Bioinformatic and experimental approaches. Microb. Cell Fact., 23, Article 190. https://doi.org/10.1186/s12934-024-02463-5

18. Bradford, M. M. (1976) A rapid and sensitive method for the quantitation of microgram quantities of protein utilizing the principle of protein–dye binding. Anal. Biochem., 72, 248–254. https://doi.org/10.1016/0003-2697(76)90527-3

19. Steyert, S. R., and Kaper, J. B. (2012) Contribution of urease to colonization by Shiga toxin-producing *Escherichia coli*. Infect. Immun., 80(8), 2589–2600. https://doi.org/10.1128/IAI.00210-12

20. Arumugam, H. R., Chattopadhyay, A., Zaroliwalla, D., Sanghavi, D., Gupta, E., Jha, N., and Reshamwala, S. (2026) Biological carbon capture using spinach carbonic anhydrase immobilized on magnetite nanoparticles. Sustainability & Circularity NOW, 2, a27973446. https://doi.org/10.1055/a-2797-3446

21. Wilbur, K. M., and Anderson, N. G. (1948) Electrometric and colorimetric determination of carbonic anhydrase. J. Biol. Chem., 176, 147–154. https://doi.org/10.1016/S0021-9258(18)51011-5

22. Laemmli, U. K. (1970) Cleavage of structural proteins during the assembly of the head of bacteriophage T4. Nature, 227, 680–685. https://doi.org/10.1038/227680a0

685 23. Edwards, L. J., and Patton, R. L. (1966) Visualization of carbonic anhydrase activity in
686 polyacrylamide gels. Stain Technol., 41, 333–334. https://doi.org/10.3109/10520296609116335

687 24. Stepanović, S., Vuković, D., Hola, V., Di Bonaventura, G., Djukić, S., Ćirković, I., and Ruzicka,
688 F. (2007) Quantification of biofilm in microtiter plates: Overview of testing conditions and
689 practical recommendations for assessment of biofilm production by staphylococci. APMIS, 115,
690 891–899. https://doi.org/10.1111/j.1600-0463.2007.apm_630.x

691 25. Dhami, N. K., Reddy, M. S., and Mukherjee, A. (2014) Synergistic role of bacterial urease and
692 carbonic anhydrase in carbonate mineralization. Appl. Biochem. Biotechnol., 172, 2552–2561.
693 https://doi.org/10.1007/s12010-013-0694-0

694 26. Lane, D. J. (1991) 16S/23S rRNA sequencing. in Nucleic Acid Techniques in Bacterial
695 Systematics (Stackebrandt, E. and Goodfellow, M., eds.), Wiley, Chichester, pp. 115–175.

696 27. Hall, T. A. (1999) BioEdit: A user-friendly biological sequence alignment editor and analysis
697 program for Windows 95/98/NT. Nucleic Acids Symp. Ser., 41, 95–98.

698 28. Altschul, S. F., Gish, W., Miller, W., Myers, E. W., and Lipman, D. J. (1990) Basic local
699 alignment search tool. J. Mol. Biol., 215(3), 403–410. https://doi.org/10.1016/S0022-
700 2836(05)80360-2

701 29. Thompson, J. D., Higgins, D. G., and Gibson, T. J. (1994) CLUSTAL W: Improving the
702 sensitivity of progressive multiple sequence alignment through sequence weighting, position-
703 specific gap penalties and weight matrix choice. Nucleic Acids Res., 22(22), 4673–4680.
704 https://doi.org/10.1093/nar/22.22.4673

705 30. Kumar, S., Stecher, G., Suleski, M., Sanderford, M., Sharma, S., and Tamura, K. (2024)
706 MEGA12: Molecular evolutionary genetic analysis version 12 for adaptive and green computing.
707 Mol. Biol. Evol., 41(12), msae263. https://doi.org/10.1093/molbev/msae263

31. Tamura, K. (1992) Estimation of the number of nucleotide substitutions when there are strong transition-transversion and G+C-content biases. Mol. Biol. Evol., 9(4), 678–687. https://doi.org/10.1093/oxfordjournals.molbev.a040752

32. Saitou, N., and Nei, M. (1987) The neighbor-joining method: A new method for reconstructing phylogenetic trees. Mol. Biol. Evol., 4(4), 406–425. https://doi.org/10.1093/oxfordjournals.molbev.a040454

33. Felsenstein, J. (1985) Confidence limits on phylogenies: An approach using the bootstrap. Evolution, 39(4), 783–791. https://doi.org/10.1111/j.1558-5646.1985.tb00420.x

34. Janda, J. M., and Abbott, S. L. (2007) 16S rRNA gene sequencing for bacterial identification in the diagnostic laboratory: Pluses, perils, and pitfalls. J. Clin. Microbiol., 45(9), 2761–2764. https://doi.org/10.1128/JCM.01228-07

35. Said, D., Ibrahim, S. M., Heikal, M., Abdel-Monem, M. O., and Dawwam, G. E. (2025) Bio-mineralization process of $CaCO_3$ induced by bacteria isolated from Egypt for sustainable bio-concrete. Microb. Cell Fact., 24, 203. https://doi.org/10.1186/s12934-025-02837-3

36. Shiri, M., Bahari, A., Khani Sarbangholi, M. M., Vatin, N. I., Rahmani, H., Ebrahimpour Bozorg, A., Gholamian, E., and Kordlou, M. (2026) Microbial-induced calcite precipitation by indigenous alkaliphilic bacteria: A dual-enzyme strategy for crack-healing in cementitious materials. Appl. Microbiol. Biotechnol., 110, 93. https://doi.org/10.1007/s00253-026-13764-7

37. Lu, S., Wang, J., Chitsaz, F., Derbyshire, M. K., Geer, R. C., Gonzales, N. R., Gwadz, M., Hurwitz, D. I., Marchler, G. H., Song, J. S., Thanki, N., Yamashita, R. A., Yang, M., Zhang, D., Zheng, C., Lanczycki, C. J., and Marchler-Bauer, A. (2020) CDD/SPARCLE: The conserved domain database in 2020. Nucleic Acids Res., 48(D1), D265–D268. https://doi.org/10.1093/nar/gkz991

731 38. Paysan-Lafosse, T., Blum, M., Chuguransky, S., Grego, T., Pinto, B. L., Salazar, G. A., *et al*.
732 (2023) InterPro in 2022. Nucleic Acids Res., 51(D1), D418–D427.
733 https://doi.org/10.1093/nar/gkac993

734 39. Jumper, J., Evans, R., Pritzel, A., Green, T., Figurnov, M., Ronneberger, O., *et al*. (2021) Highly
735 accurate protein structure prediction with AlphaFold. Nature, 596, 583–589.
736 https://doi.org/10.1038/s41586-021-03819-2

737 40. Pettersen, E. F., Goddard, T. D., Huang, C. C., Meng, E. C., Couch, G. S., Croll, T. I., Morris, J.
738 H., and Ferrin, T. E. (2021) UCSF ChimeraX: Structure visualization for researchers, educators,
739 and developers. Protein Sci., 30(1), 70–82. https://doi.org/10.1002/pro.3943

740 41. Hurlbert, S. H. (1984) Pseudoreplication and the design of ecological field experiments. Ecol.
741 Monogr., 54, 187–211. https://doi.org/10.2307/1942661

742 42. Lazic, S. E. (2010) The problem of pseudoreplication in neuroscientific studies: Is it affecting
743 your analysis? BMC Neurosci., 11, Article 5. https://doi.org/10.1186/1471-2202-11-5

744 43. Montgomery, D. C. (2017) Design and analysis of experiments (9th ed.). Wiley.

745 44. Lakens, D. (2013) Calculating and reporting effect sizes to facilitate cumulative science: A
746 practical primer for t-tests and ANOVAs. Front. Psychol., 4, 863.
747 https://doi.org/10.3389/fpsyg.2013.00863

748 45. Tukey, J. W. (1949) Comparing individual means in the analysis of variance. Biometrics, 5, 99–
749 114. https://doi.org/10.2307/3001913

750 46. Shapiro, S. S., and Wilk, M. B. (1965) An analysis of variance test for normality (complete
751 samples). Biometrika, 52, 591–611. https://doi.org/10.1093/biomet/52.3-4.591

752 47. Brown, M. B., and Forsythe, A. B. (1974) Robust tests for the equality of variances. J. Am. Stat.
753 Assoc., 69, 364–367. https://doi.org/10.1080/01621459.1974.10482955

754 48. Holm, S. (1979) A simple sequentially rejective multiple test procedure. Scand. J. Stat., 6, 65–
755 70.

49. Virtanen, P., Gommers, R., Oliphant, T. E., Haberland, M., Reddy, T., Cournapeau, D., *et al*. (2020) SciPy 1.0: Fundamental algorithms for scientific computing in Python. Nat. Methods, 17, 261–272. https://doi.org/10.1038/s41592-019-0686-2

50. Seabold, S., and Perktold, J. (2010) Statsmodels: Econometric and statistical modeling with Python. In S. van der Walt and J. Millman (Eds.), Proceedings of the 9th Python in Science Conference (pp. 92–96). https://doi.org/10.25080/Majora-92bf1922-011

51. Achal, V., and Pan, X. (2011) Characterization of urease and carbonic anhydrase producing bacteria and their role in calcite precipitation. Curr. Microbiol., 62, 894–902. https://doi.org/10.1007/s00284-010-9801-4

52. Naja, K., Alhadidi, S. H., Elsayed, H., Al-Khayat, J. A. A., Sadooni, F., Al-Kuwari, H. A. S., and Al Disi, Z. A. (2025) Characterizing carbonate mineral-forming bacterial strains and their carbonic anhydrase activities in two coastal sabkhas. Biochem. Biophys. Rep., 43, 102064. https://doi.org/10.1016/j.bbrep.2025.102064

53. Del Prete, S., De Luca, V., Iandolo, E., Supuran, C. T., and Capasso, C. (2015) Protonography, a powerful tool for analyzing the activity and the oligomeric state of the γ-carbonic anhydrase identified in the genome of *Porphyromonas gingivalis*. Bioorg. Med. Chem., 23, 3747–3750. https://doi.org/10.1016/j.bmc.2015.03.080

54. Nathan, V. K., Vijayan, J., and Parvathi, A. (2020) Optimization of urease production by *Bacillus halodurans* PO15: A mangrove bacterium from Poovar mangroves, India. Mar. Life Sci. Technol., 2, 194–202. https://doi.org/10.1007/s42995-020-00031-5

55. Hoffmann, T. D., Paine, K., and Gebhard, S. (2021) Genetic optimisation of bacteria-induced calcite precipitation in *Bacillus subtilis*. Microb. Cell Fact., 20, 214. https://doi.org/10.1186/s12934-021-01704-1

56. Sharma, B., Sharma, S., Medicherla, K. M., and Reddy, S. M. (2024) Genome sequence analysis of calcifying bacteria *Bacillus paranthracis* CT5 and its biomineralization efficacy to improve

the strength and durability properties of civil structures. Curr. Microbiol., 81, 109. https://doi.org/10.1007/s00284-024-03625-9

57. Zhu, Y., Ma, N., Jin, W., Wu, S., and Sun, C. (2017) Genomic and transcriptomic insights into calcium carbonate biomineralization by marine actinobacterium *Brevibacterium linens* BS258. Front. Microbiol., 8, 602. https://doi.org/10.3389/fmicb.2017.00602

58. Ma, Z., Chen, M., Lu, J., Liu, S., and Ma, Y. (2025) Exploration of urease-aided calcium carbonate mineralization by enzyme analyses of *Neobacillus mesonae* strain NS-6. Microbiol. Spectr., 13(1), e01891-24. https://doi.org/10.1128/spectrum.01891-24

59. Okshevsky, M., Regina, V. R., and Meyer, R. L. (2015) Extracellular DNA as a target for biofilm control. Curr. Opin. Biotechnol., 33, 73–80. https://doi.org/10.1016/j.copbio.2014.12.002

60. Tuttle, M. J., Bradow, B. M., Martineau, R. L., Carter, M. S., Mancini, J. A., Holley, K. A., Diltz, R. A., Hung, C.-S., and Gupta, M. K. (2025) Shelf-stable *Sporosarcina pasteurii* formulation for scalable laboratory and field-based production of biocement. ACS Appl. Mater. Interfaces, 17(5), 7251–7261. https://doi.org/10.1021/acsami.4c15381

61. Mwandira, W., Mavroulidou, M., Satheesh, A., Gunn, M. J., Gray, C., Purchase, D., and Garelick, J. (2023) An electrokinetic-biocementation study for clay stabilisation using carbonic anhydrase-producing bacteria. Environ. Sci. Pollut. Res., 30, 104916–104931. https://doi.org/10.1007/s11356-023-29817-7

62. Sharma, A., Bhattacharya, A., Pujari, R., and Shrivastava, A. (2008) Characterization of carbonic anhydrase from diversified genus for biomimetic carbon-dioxide sequestration. Indian J. Microbiol., 48, 365–371. https://doi.org/10.1007/s12088-008-0045-y

63. Abdel-Aleem, H., Dishisha, T., Saafan, A., AbouKhadra, A. A., and Gaber, Y. (2019) Biocementation of soil by calcite/aragonite precipitation using *Pseudomonas azotoformans* and *Citrobacter freundii* derived enzymes. RSC Adv., 9, 17601–17611. https://doi.org/10.1039/C9RA02247C

Statements and Declarations

Funding

The authors declare that no specific funding was received for this study.

Competing Interests

All authors declare that they have no actual or potential competing financial interests or personal relationships that could have influenced the work reported in this original research paper.

Ethics Approval

Not applicable. This study involves environmental bacterial isolates and does not involve human participants or animal models.

Consent to Participate

Not applicable.

Consent for Publication

All authors consent to publish this manuscript.

Availability of Data and Material:

Data will be made available on request.

Authors' Contributions

Paul M. conceptualized the study, developed the methodology, and wrote the original draft. Parvathi A. and Vinod K. assisted with process optimization and data analysis. Neenu P. and Suhara A. contributed to the biochemical assays and microbiology experiments. Parvathi A. also provided supervision, resources, and reviewed and edited the final manuscript. All authors read and approved the final version.

Supplementary Files

This is a list of supplementary files associated with this preprint. Click to download.

- Supplementarymaterials.docx